Korean J. Chem. Eng., **30**(3), 620-625 (2013)
DOI: 10.1007/s11814-012-0189-7

Improved electrochemical performance of dye-sensitized solar cell via surface modifications of the working electrode by electrodeposition

Kang-Il Jang, Eunpyo Hong, and Jung Hyeun Kim†

Department of Chemical Engineering, University of Seoul, Seoul 130-743, Korea
(*Received 26 August 2012 • accepted 3 November 2012*)

Abstract−Modifications of the working electrode with TiO_2 blocking or coating layers are carried by electrodeposition in $TiCl_3$ precursor solution. The results suggest that the electrodeposited TiO_2 blocking layer provides excellent agglutination between the FTO substrate and the active TiO_2 layer. In addition, the electrodeposited TiO_2 coating layer enhances the interconnections between the TiO_2 nanoparticles and the FTO substrate, and therefore it increases the electron transport efficiency. The morphology and crystalline structure of the electrodeposited TiO_2 layers are characterized by SEM, TEM, and XRD. The electrochemical impedance spectroscopy measurements show that the improved DSSC performance with the electrodeposited coating layer is mainly due to the increase in the lifetime of the conduction band electron in the TiO_2 film. The photoelectron conversion efficiency of DSSC is increased from 3.47% to 5.38% by employing the TiO_2 electrodeposited working electrode.

Key words: DSSC, TiO_2, Blocking Layer, Electrodeposition

INTRODUCTION

There has been increasing demand for appropriate alternative energy sources. The conversion of solar radiation to electricity has become increasingly important because sunlight is a clean and limitless energy source compared to traditional fossil energy sources [1-5]. DSSCs can be produced at low-cost with widely usable materials and easily accessible manufacturing equipment. On the other hand, DSSCs have the problem of a relatively low conversion efficiency compared to silicon-based solar cells. One of the important issues to increase the cell efficiency is a suitable structure of the porous TiO_2 film to increase the level of dye adsorption and to minimize the electron loss through the cell circuit.

DSSCs are composed mainly of three parts: a dye sensitized nanocrystalline film as a photo anode, an iodide/triiodide (I^-/I_3^-) redox electrolyte, and a platinum-coated transparent conducting oxide (TCO) glass as a counter electrode. The electrons excited from the dye are transferred step by step through the conducting band of TiO_2 nanocrystallites and FTO electrode. The dye is regenerated by electron donation from the redox system of the electrolyte. The iodide is recovered by the reduction of triiodide on the platinum layer of the counter electrode. In practice, the FTO surface might not be fully covered with the mesoporous TiO_2 film due to the porous nature of the TiO_2 film. The exposed surface area of the FTO to the electrolyte may lead to charge recombination between the TiO_2 and the FTO interfaces. Electron transfer to the FTO is possibly intercepted by the reduction of the electrolyte interacting with the electrode. Another weakness of mesoporous TiO_2 films is the inadequate connection between TiO_2 nanoparticles, leading to an increase in electron transfer resistance [6-8]. To solve this recombination and electron transfer resistance problem, previous studies have demonstrated that it is effective to introduce a compact and thin TiO_2 blocking layer onto the transparent conducting glass substrate [9-11] using a range of preparation methods such as sputtering [11,12], sol-gel [13, 14], and spray-coating [15,16] techniques. A $TiCl_4$ post-treatment of the TiO_2 photoanode is a common modification method for obtaining a reliable thin TiO_2 coating layer to improve the cell performance such as current density, fill factor, and conversion efficiency [17-19].

In this study, an electrodeposition strategy was used to modify the mesoporous TiO_2 photoanode in two schemes: i) a blocking layer prepared first by the electrodeposition on the FTO substrate and then TiO_2 photoanode fabricated, and ii) a TiO_2 photoanode fabricated first and then the electrodeposition performed for covering the interfaces on the FTO substrate and mesopores between TiO_2 nanoparticles. Experimental parameters for TiO_2 electrodeposition were applied voltage and electrodeposition time. The blocking layer can reduce the electron recombination phenomena from FTO to electrolyte by separating effectively at a specific layer thickness [20]. In addition, a thin TiO_2 coating layer formed by the electrodeposition can not only reduce electron recombination from FTO to electrolyte, but also increase electron transport between TiO_2 nanoparticles because the $TiCl_3$ precursor solution can penetrate deep into the exposed FTO surface and the mesoporous TiO_2 nanoparticles. The photovoltaic properties of the DSSCs with the TiO_2 modified photo anode by electrodeposition were characterized and compared with those of the unmodified photo anode case.

EXPERIMENTAL

1. Materials

The 20 wt% $TiCl_3$ solution for electrodeposition was purchased from Alfa Aesar Co. Ltd. (USA). The colloidal TiO_2 paste for the doctor blade was obtained by adding 0.375 g polyethylene oxide (PEO, Sigma-Aldrich), 1.5 g TiO_2 particles (P25, Degussa) and 0.3

†To whom correspondence should be addressed.
E-mail: jhkimad@uos.ac.kr

ml Triton X-100 (Sigma-Aldrich) into 20 ml mixed solution of deionized (DI) water and ethanol (50 : 50 ratio). The solution was stirred for 24 h and kept at room temperature for further use. H_2PtCl_6 (Sigma-Aldrich), N719 (Solaronix), I^-/I_3^- electrolyte (HC-DII, TG-energy) were also used for cell fabrications. FTO conducting glass (18 Ω/cm^2) was used for substrate.

2. Electrodeposition of the TiO_2 Blocking and Coating Layers

Before electrodeposition, the FTO glass was dipped in a solution of ethanol and acetone (50 : 50 ratio), and cleaned thoroughly with ultrasonication in DI water. To prepare the TiO_2 blocking layer, a 16 vol %$TiCl_3$ electrolyte solution was prepared by diluting with DI water, and the pH of the solution was adjusted to 2.1-2.2 to increase the deposition efficiency as reported elsewhere [21]. Three-electrode electrochemical cells were equipped with a Pt-mesh counter electrode, an Ag/AgCl reference electrode, and an FTO conducting glass (1.5×1.5 cm^2) as an working electrode. The working voltage ranged from 0.1 V to 1.0 V using a potentiostat (Iviumstat, Netherland) for various deposition time periods. After the electrodeposition, the substrates were washed with ethanol and sintered for 30 min at 450 °C. The same process for the TiO_2 coating layer formation was repeated with the reference electrode made by a doctor blade method.

3. Fabrication of DSSCs

The working electrodes (reference, including the blocking layer, and including the coating layer) were made with the TiO_2 paste using a doctor blade method, and they were sintered at 450 °C for 30 min. The TiO_2 film thickness of the working electrode was approximately 17 μm. The photoactive area of the prepared electrodes was 25 mm^2 (5 mm×5 mm). Dye adsorption was carried out by dipping the TiO_2 electrode in a dye solution at room temperature for 24 h. The working electrode was then washed, dried, and used for cell fabrications. The counter electrodes were prepared by placing a few drops of a 0.007 M H_2PtCl_6 isopropanol solution on the FTO substrates and by sintering at 450 °C for 30 min. A sandwich cell was prepared using the dye-adsorbed electrode as the working electrode and a platinum-coated conducting glass electrode as the counter electrode. The cell was sealed with Surlyn resin (Peccell-Technologies) between the two electrodes by heat treatment at 90 °C for 30 seconds. Finally, the electrolyte solution was introduced into the inter electrode space from the counter electrode side through a predrilled hole. The hole was sealed with the Surlyn resin to avoid leakage of the electrolyte solution.

4. Measurements

X-ray diffraction (XRD, D/MAX 2500, Japan) was performed for crystalline structure analysis of the TiO_2 nanoparticles, the TiO_2 blocking and coating layers using Cu Kα radiation. Scanning electron microscope (SEM, SUPRA 55VP, Germany) was used to observe the surface morphology. Transmission electron microscopy (TEM, G2F30ST, Netherland) image was operated at 300 kV. The incident photon to current conversion efficiency (IPCE) as a function of the excitation wavelength was obtained at a low chopping speed of 10 Hz under a white-light bias using a system designed by PV measurements. A 75 W Xenon lamp was applied as the light source for the monochromatic beam. A silicon photodiode (NIST-calibrated photodiode G425) was used for calibration. The open-circuit voltage V_{oc} (V), short-circuit current density J_{sc} (mW/cm^2), fill factor (%) and energy conversion efficiency (%) of the DSSCs were measured using a solar simulator (PEC-L11, Japan) and a potentiostat (Iviumstat, Netherland), and the light source was a 100 W Xenon lamp with a light density of AM 1.5 (100 mW/cm^2). The electrochemical impedance spectroscopy was also performed using the potentiostat.

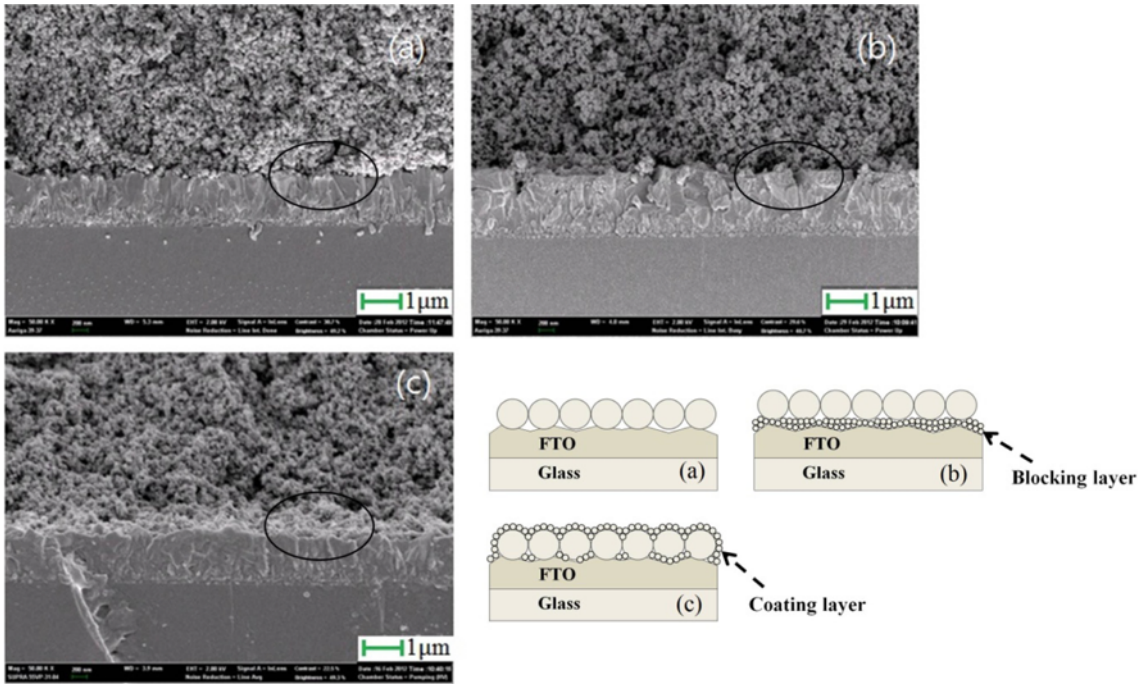

Fig. 1. Cross-sectional SEM images from (a) the reference electrode, (b) including the electrodeposited TiO_2 blocking layer, and (c) including the electrodeposited TiO_2 coating layer.

RESULTS AND DISCUSSION

Fig. 1 shows cross-sectional SEM images including schematic illustrations of the various interfaces between the TiO_2 nanoparticles and the FTO substrates. As schematically explained, the FTO substrate is directly contacted with the TiO_2 nanoparticle film if there is no electrodeposition performed (Fig. 1(a)). On the other hand, a blocking layer is formed between the TiO_2 nanoparticle film and the FTO substrate (Fig. 1(b)), and the thin coating layer covers TiO_2 nanoparticles and the FTO surface (Fig. 1(c)). The thin coating layer could increase electron transport properties through nanoparticles by forming a compact TiO_2 layer on the FTO substrate and bridging the TiO_2 interconnections between the TiO_2 nanoparticles.

Fig. 2 shows transmission electron microscopy (TEM) images of the TiO_2 nanoparticles: (a) P25 itself and (b) P25 including electrodeposited nanoparticles in the coating layer. The average size of the P25 TiO_2 nanoparticles is revealed to be about 25 nm, as suggested from the provider [22]. However, the size of the electrodeposited nanoparticles from the coating layer was approximately smaller than 10 nm. In addition, the TiO_2 nanoparticles in the coating layer fill most of the empty spaces between the P25 nanoparticles as also demonstrated in Fig. 1(c), and thus the electrodeposited TiO_2 increase the interconnections between the TiO_2 nanoparticles and with the FTO substrate. As a result, the electrodeposited layer would improve electron transports through the cell circuit.

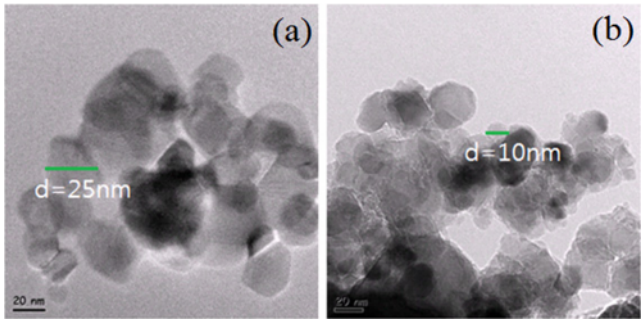

Fig. 2. TEM images of the P25 TiO_2 nanoparticles (a) and the P25 particles including the electrodeposited TiO_2 nanoparticles (b).

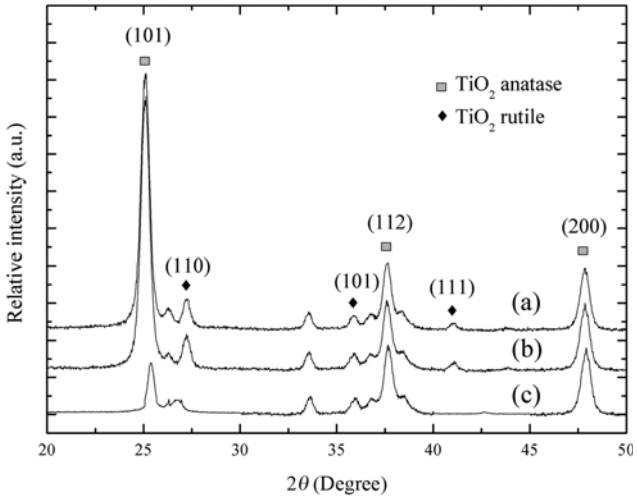

Fig. 3. XRD patterns measured from the reference P25 TiO_2 nanoparticles (a), including the TiO_2 coating layer (b), and the only electrodepositedTiO_2 nanoparticles from the blocking layer (c).

Fig. 3 shows the X-ray diffraction patterns of only the TiO_2 nanoparticles, the only electrodeposited blocking layer, and TiO_2 nanoparticles including the coating layer. The characteristic peaks of the blocking layer show weakly mixed phases of anatase and rutile structures, and the peak intensities including TiO_2 nanoparticles are much strong in the same diffraction angles. It is because the TiO_2 nanoparticle layer (~20 μm) is much thicker than the blocking layer (~400 nm). With the same crystalline material characteristic, there would be no electron transfer resistance between the blocking layer surface and the TiO_2 nanoparticles. In the same sense for the coating layer formed by electrodeposition, it would further reduce electron losses between TiO_2 nanoparticles and through the circuit by the dense packing.

Fig. 4 shows the photocurrent-voltage (J-V) characteristics of the DSSCs for three different cases. From these J-V measurement results, the photovoltaic parameters and the cell efficiencies are summarized in Table 1. The short-circuit current densities (J_{sc}) from the blocking and the coating layers were increased by 21.2% and 57.4%, respectively, compared to the reference working electrode case. This increment of the current density demonstrates that the electron transfer resistance is much reduced by introducing the additional layers by electrodeposition. The change of V_{oc} is not noticeable, but the value of V_{oc} is slightly changed after the electrodeposition process

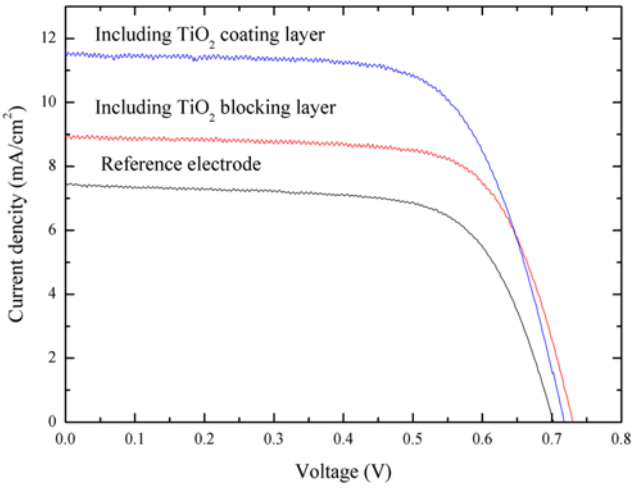

Fig. 4. Photocurrent-voltage (J-V) characteristics of the DSSCs employing the reference electrode, including the electrodeposited TiO_2 blocking layer, and including the electrodeposited TiO_2 coating layer.

Table 1. Photovoltaic cell parameters analyzed from the J-V measurements

Cell	J_{sc} ($mAcm^{-2}$)	V_{oc} (V)	FF (%)	η (%)
Including the coating layer	11.54	0.71	0.65	5.38
Including the blocking layer	8.88	0.73	0.68	4.44
Reference electrode	7.33	0.70	0.67	3.47

compared to the reference electrode case. It is possibly due to the reduced recombination of the photo generated electron-hole pairs by the additional electrodeposited layer. However, the V_{oc} in case of the coating layer is slightly decreased compared to the blocking layer case. It may come from the coverage difference of TiO_2 particles formed on the FTO surface between the blocking layer and the coating layer. In addition, the photoelectron conversion efficiencies (η) of the DSSCs by employing the blocking and the coating layers were also increased by 27.9% and 55.0% due to the improvements of the photocurrent density. Generally, with an aid of the conventional $TiCl_4$ post-treatment on the TiO_2 films for DSSCs, the J_{sc} and η are increased about 10-15% and 10-20%, respectively [17,23,24]. Therefore, compared with the conventional post treatment method, the electrodeposition is an efficient way of introducing interfacial layers to improve the cell performance with increased values of J_{sc}.

In addition to the J-V characteristics of the solar cells, the electrochemical impedance spectroscopy (EIS) under one-sun illumination condition is a useful technique to analyze electron transport behavior at the nanoparticle or film interfaces [25-27]. From the EIS measurements, a spectrum for a DSSC exhibits three semicircles in the Nyquist plot (Fig. 5(a)) or three characteristic frequency peaks in the Bode phase plot (Fig. 5(b)). The typical Nyquist plot features three semicircles that in the order of increasing frequency are attributed to the diffusion within the electrolyte, the electron transfer at the TiO_2/electrolyte interfaces, and the redox reaction at the Pt counter and working electrodes [28,29]. Fig. 5(a) also includes an equivalent electrical circuit containing a constant-phase element (CPE). The resistance R_1 results from the interfacial resistances at the electrodes [30,31] and the resistance R_2 originates from the charge transfer resistance at the TiO_2/dye/electrolyte interfaces [32-34]. R_s and R_3 are attributed to the resistances from the FTO substrate itself and electrolyte diffusion. The R_1 and R_2 values of the reference DSSC were calculated to be approximately 7.6 and 19.2, which are much higher than those with electrodeposited TiO_2 blocking and coating layers (summarized in Table 2). Clearly, the R_1 was reduced significantly after modifying the photo anode due to decreased interfacial resistance by electrodeposition at the working electrode. The R_2 was dominantly reduced with the TiO_2 coating layer, and it is also attributed to the increased interfacial contacts between TiO_2 nanoparticles and with the electrolyte.

From the Bode phase plot, the electron recombination lifetime (τ_r) in the TiO_2 electrode can be estimated from the minimum angular frequency (ω_{min}) of the impedance semicircle at the peak frequencies in the spectrum, as $\tau_r=1/\omega_{min}$. Fig. 5(b) indicates that the characteristic frequency decreases with the electrodeposited TiO_2 layers; especially, it shows the lowest frequency with the coating layer. It suggested that the electron life time was increased about 6 times

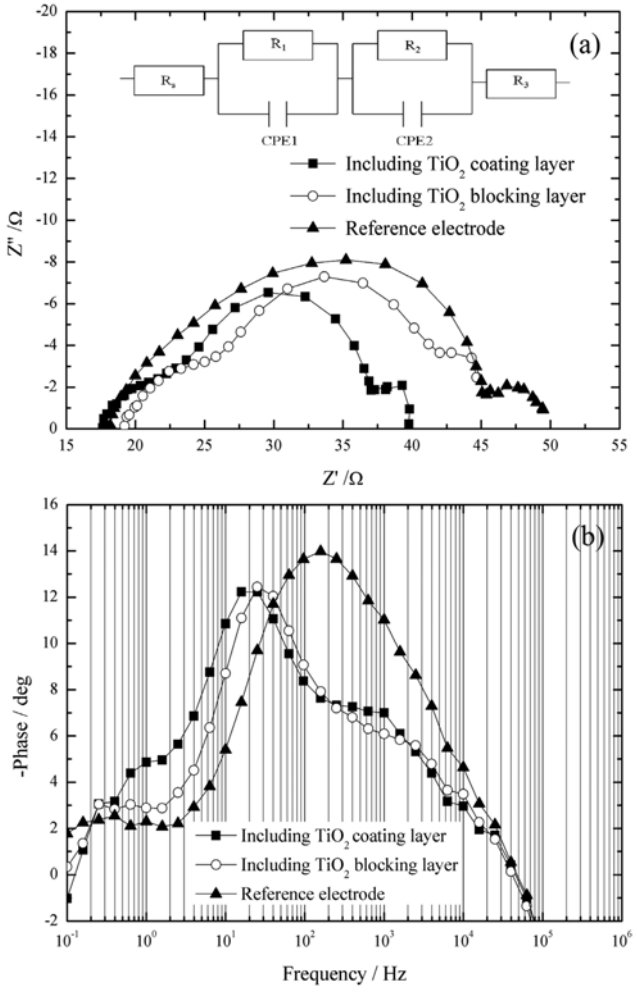

Fig. 5. Nyquist plots (a) and Bode phase plots (b) from the DSSCs with the reference electrode, including the electrodeposited TiO_2 blocking layer, and including the electrodeposited TiO_2 coating layer ($R_{1,2,3}$: resistance unit, CPE 1, 2: constant-phase element unit).

Table 2. Resistance (R_s, R_1, and R_2), minimum angular frequency (ω_{min}) and electron recombination life times (τ_r)

Cell	R_1/Ω	R_2/Ω	R_3/Ω	ω_{min}/Hz	τ_r/ms
Including the coating layer	23.16	37.02	40.08	25.12	39.80
Including the blocking layer	25.18	42.15	44.91	39.81	25.12
Reference electrode	25.82	45.06	49.56	158.50	6.31

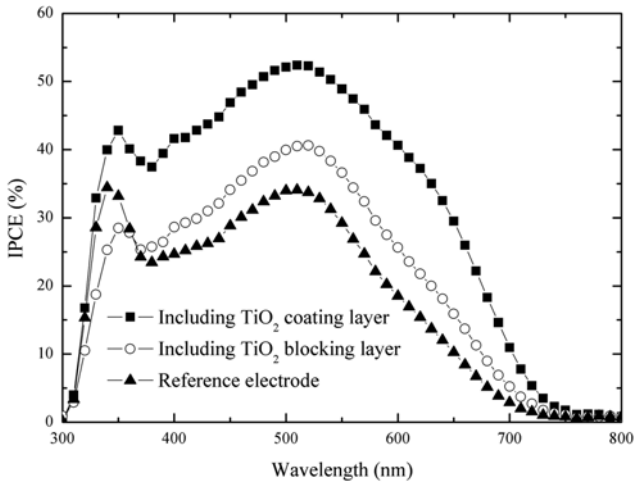

Fig. 6. IPCE spectra from the DSSCs with the reference electrode, including the electrodeposited TiO_2 blocking layer, and including the electrodeposited TiO_2 coating layer.

with the electrodeposited TiO_2 coating layer. Table 2 summarizes the electrochemical parameters (R_s, R_1, and R_2), minimum angular frequency (ω_{min}), and electron recombination lifetimes (τ). Therefore, the EIS measurements showed that the improved DSSC performance was mainly due to the increase in the lifetime of the conduction band electron in the TiO_2 film.

Fig. 6 shows the IPCE (incident photon to current conversion efficiency) spectra of the DSSCs with a reference electrode, with an electrodeposited TiO_2 blocking layer, and with an electrodeposited TiO_2 coating layer. There are three major factors affecting the IPCE of a DSSC as follows [35,36]:

$$IPCE=LHE\times\phi_{inj}\times\eta_{coll}$$

where LHE is the light harvesting efficiency which is related to the incident light absorbed by the dye molecules, ϕ_{inj} is the electron injection efficiency from the excited electron in dye molecules into TiO_2 conduction band, and η_{coll} is the collection efficiency of the injected electrons to the FTO substrate. The LHE is closely related to the amount of the dye loading on the TiO_2 photoelectrode. In this study, the amounts of dye loading (7.1×10^{-8} mol/cm^2 with the reference electrode, 7.0×10^{-8} mol/cm^2 including the blocking layer, 7.3×10^{-8} mol/cm^2 including the coating layer) were similar, and so the parameters LHE and ϕ_{inj} can be considered as the same. In keeping the same TiO_2 reference electrode thickness, the blocking layer does not create additional surface area for the TiO_2 film, but the coating layer can form additional TiO_2 particles inside the TiO_2 film. Therefore, the adsorbed dye amount in the blocking layer case shows very similar value with the reference electrode, but that in the coating layer case has slightly higher value than the reference case. The η_{coll} is a dominating factor for the IPCE improvement. The IPCE with the TiO_2 coating layer shows the highest level through all wavelengths, and it may be due to the formation of a more compact connection between TiO_2 nanoparticles and with the FTO substrate [37, 38]. It results in further preventing electron recombination reactions effectively. This IPCE result with the TiO_2 coating layer coincides well with the increased electron lifetime (in Fig. 5(b) and Table 2) and reduced electron transfer resistance (in Fig. 5(a) and Table 2).

CONCLUSIONS

A three electrode deposition system was used to modify the TiO_2 photoanode. The $TiCl_3$ precursor solution permeates into the voids of the TiO_2 nanoparticles. When an anodic current was applied, electrodeposition occurred at the interfaces between the electrolyte and TiO_2 nanoparticles or FTO substrates, resulting in the layer formations on the TiO_2 nanoparticles and FTO substrate. The TiO_2 working electrodes modified with a blocking or coating layers were fabricated for effective electron transports. The EIS measurements indicated that the electrical contact resistance was significantly reduced at the interfaces shown from the Nyquist plots, and the electron recombination lifetime (6.3 ms to 39.8 ms) was increased about 6 times, shown from the Bode phase plots. In addition, the electrodeposited TiO_2 coating layer exhibited the highest IPCE spectrum, and it is due to the effective preventing the electron recombination with a more compact connection between TiO_2 nanoparticles and with the FTO substrate. It also showed the highest cell efficiency (5.38%) compared to the reference electrode case (3.47%).

ACKNOWLEDGEMENT

This work was partially supported by a grant (Code No. 2010 T100200225) from Korea Institute of Energy Technology Evaluation and Planning under the Energy R&D Programs of the Ministry of Knowledge and Economy, Korea.

REPERENCES

1. Q. Zhang and G. Cao, *Nano Today* (2011).
2. M. Gratzel, *J. Photochem. Photobiol. C: Photochem. Reviews*, **4**, 145 (2003).
3. E. Hong, J. H. Kim and S. Yu, *Korean J. Chem. Eng.*, 1 (2011).
4. J. Qi, X. Dang, P. T. Hammond and A. M. Belcher, *ACS Nano*, **5**, 7108 (2011).
5. F. Sauvage, D. Chen, P. Comte, F. Huang, L. P. Heiniger, Y. B. Cheng, R. A. Caruso and M. Graetzel, *ACS Nano*, **4**, 4420 (2010).
6. J. K. Koh, J. Kim, B. Kim, J. H. Kim and E. Kim, *Adv. Mater.*, (2011).
7. C. C. Yang and Y. R. Zheng, *J. Power Sources* (2011).
8. P. Sudhagar, K. Asokan, J. H. Jung, Y. G. Lee, S. Park and Y. S. Kang, *Nanoscale Res. Lett.*, 1 (2010).
9. R. Sahay, J. Sundaramurthy, P. Suresh Kumar, V. Thavasi, S. Mhaisalkar and S. Ramakrishna, *J. Solid State Chem.* (2011).
10. J. Kim, *J. Nanosci. Nanotechnol.*, **11**, 7335 (2011).
11. L. Meng and C. Li, *Nanosci. Nanotechnol. Lett.*, **3**, 181 (2011).
12. K. H. Choi, J. A. Jeong, J. W. Kang, D. G. Kim, J. K. Kim, S. I. Na, D. Y. Kim, S. S. Kim and H. K. Kim, *Sol. Energy Mater. Sol. Cells*, **93**, 1248 (2009).
13. T. Y. Cho, S. G. Yoon, S. S. Sekhon, M. G. Kang and C. H. Han, *Bullet. Korean Chem. Soc.*, **32**, 3629 (2011).
14. K. Han and J. H. Kim, *Mater. Lett.*, **65**, 2466 (2011).
15. R. Maric, R. Neagu, Y. Zhang-Steenwinkel, F. P. F. Van Berkel and B. Rietveld, *J. Power Sources*, **195**, 8198 (2010).
16. X. H. Chan, J. Robert Jennings, M. Anower Hossain, K. Koh Zhen Yu and Q. Wang, *J. Electrochem. Soc.*, **158**, H733 (2011).
17. H. Choi, C. Nahm, J. Kim, J. Moon, S. Nam, D. R. Jung and B. Park, *Current Appl. Phys.*, **12**, 737 (2012).
18. D. K. Roh, R. Patel, S. H. Ahn, D. J. Kim and J. H. Kim, *Nanoscale*, **3**, 4162 (2011).
19. S. Yahav, S. Rühle, S. Greenwald, H. N. Barad, M. Shalom and A. Zaban, *J. Phys. Chem. C*, **115**, 21481 (2011).
20. K. I. Jang, E. Hong and J. H. Kim, *Korean J. Chem. Eng.*, **29**(3), 356 (2012).
21. C. Lokhande, S. K. Min, K. D. Jung and O. S. Joo, *J. Mater. Sci.*, **39**, 6607 (2004).
22. J. Cunningham and P. Sedlák, *J. Photochem. Photobiol. A: Chemistry*, **77**, 255 (1994).
23. L. Vesce, R. Riccitelli, G. Soscia, T. M. Brown, A. Di Carlo and A. Reale, *J. Non-Crystalline Solids*, **356**, 1958 (2010).
24. S. Yahav, S. Rühle, S. Greenwald, H. N. Barad, M. Shalom and A. Zaban, *J. Phys. Chem. C*, **115**, 21481 (2011).
25. L. Kavan, J. H. Yum and M. Grätzel, *ACS Nano*, **5**, 165 (2011).
26. L. Kavan, J. H. Yum, M. K. Nazeeruddin and M. Grätzel, *ACS Nano*, **5**, 9171 (2011).
27. R. Kern, R. Sastrawan, J. Ferber, R. Stangl and J. Luther, *Electrochim. Acta*, **47**, 4213 (2002).

28. S. C. Yang, D. J. Yang, J. Kim, J. M. Hong, H. G. Kim, I. D. Kim and H. Lee, *Adv. Mater.*, **20**, 1059 (2008).
29. J. P. Diard and C. Montella, *J. Electroanal. Chem.*, **557**, 19 (2003).
30. S. Lee, J. H. Noh, H. S. Han, D. K. Yim, D. H. Kim, J. K. Lee, J. Y. Kim, H. S. Jung and K. S. Hong, *J. Phys. Chem. C*, **113**, 6878 (2009).
31. K. Miettunen, J. Halme, P. Vahermaa, T. Saukkonen, M. Toivola and P. Lund, *J. Electrochem. Soc.*, **156**, B876 (2009).
32. Q. Wang, J. E. Moser and M. Grätzel, *J. Phys. Chem. B*, **109**, 14945 (2005).
33. L. Han, N. Koide, Y. Chiba, A. Islam and T. Mitate, *Comptes Rendus Chimie*, **9**, 645 (2006).
34. N. Koide, A. Islam, Y. Chiba and L. Han, *J. Photochem. Photobiol. A: Chemistry*, **182**, 296 (2006).
35. Q. Yu, Y. Wang, Z. Yi, N. Zu, J. Zhang, M. Zhang and P. Wang, *ACS Nano*, **4**(10), 6032 (2010).
36. S. R. Jang, K. Zhu, M. J. Ko, K. Kim, C. Kim, N. G. Park and A. J. Frank, *ACS Nano*, **5**(10), 8267 (2011).
37. P. Sommeling, B. O'regan, R. Haswell, H. Smit, N. Bakker, J. Smits, J. Kroon and J. Van Roosmalen, *J. Phys. Chem. B*, **110**, 19191 (2006).
38. G. D. Sharma, P. Suresh and J. A. Mikroyannidis, *Electrochim. Acta*, **55**, 2368 (2010).